Water sorption equilibrium on 2-Hydroxyethyl-trimethylammonium acetate in the temperature range 298.25349.55 K

Water sorption equilibrium on 2-Hydroxyethyl-trimethylammonium acetate in the temperature range 298.25−349.55 K

Mauro Luberti, Christopher Olkis, Grady Bensted, Giulio Santori*

School of Engineering, Institute for Materials and Processes, The University of Edinburgh
Sanderson Building, King's Buildings, Robert Stevenson Road, Edinburgh, EH9 3FB; Email: g.santori@ed.ac.uk

Abstract
Ionic liquids (ILs) have emerged as novel sorption materials capable to achieve exceptional water vapour uptake that is attractive for their use in heat transformation technologies. Water sorption equilibria on 2-hydroxyethyl-trimethylammonium acetate or choline acetate ([Cho][OAc]) were measured at eight different temperatures: 298.25, 303.25, 308.35, 318.55, 328.75, 333.85, 344.15 and 349.55 K. Equilibrium measurements were performed with a dynamic vapour sorption (DVS) system. With a relative humidity of around 90% a water uptake larger than 3.5 $g_W\ g_{IL}^{-1}$ was observed for all the temperatures. The resulting type III isotherms were correlated with the Guggenheim-Anderson-de Boer (GAB) model as well as the Redlich-Kister (RK) excess Gibbs energy model. It was found that both models fit the experimental data with great accuracy and provide an appropriate description of the water sorption equilibria. The regressed parameters of the RK model were also employed to predict excess properties of the binary system. Moreover, a thermodynamic cycle was assessed and compared with sorbent benchmarks, highlighting performance that make the choline acetate/water pair a viable option in sorption chiller applications.

Keywords: Water sorption equilibrium; Water vapour; Ionic liquid; Choline acetate; Guggenheim-Anderson-de Boer model; Redlich-Kister model; Sorption chiller; COP

1. Introduction
Due to global warming there is an ever-present need to increase the world's energy efficiency. Temperature swing sorption (TSS) systems can address this challenge being technologies driven by heat below 100°C [1–4]. In a TSS heat transformer, water vapour is absorbed or adsorbed onto a sorption material, either a liquid solvent, a salt or a porous solid. Typical applications include heat storage [5,6], desalination [7,8], drying [9–11] and cooling [12].
Beyond inorganic salts and conventional adsorbents, ionic liquids (ILs) have shown promising water sorption properties [13–16]. Many industrial sectors are exploring the possible uses for ILs because of their negligible vapour pressure, non-flammability, high solubility of organic compounds, high thermal and chemical stability and ease of extraction from reaction products [17,18]. Some ILs are environmentally neutral and are currently being studied to replace traditional industrial solvents [19]. Moreover, ionic liquids have a low regeneration temperature, often under 80°C, which makes them attractive for their utilization in heat transformers [8].
Despite the remarkable potential for several applications, there are only limited works in the literature focussing on water sorption equilibrium on ionic liquids. Römich et al. [20] measured several thermodynamic properties of binary mixtures of water + [EMIM][OAc] and water + [DEMA][OMs] in the temperature range 293.15−353.15 K. These properties included vapour-liquid equilibria (VLE), heat capacities, densities and viscosities. They found that the NRTL model showed a good agreement between measured and correlated data. Merkel et al. [21] studied VLE of systems of water and six ILs in order to assess and rank the influence of the cation and the anion on the vapour pressure reduction of ILs. VLE experimental data were also regressed using the NRTL model which was then used to predict excess molar enthalpies. Costantinescu et al. [22] reported viscosities, VLE and heat of mixing measurements for water with three choline-based ionic liquids at 303.15, 313.15 and 323.15 K. The experimental VLE data were correlated using the NRTL and UNIQUAC models while molar excess enthalpies were fitted to a Redlich-Kister model. Khan et al. [23] investigated VLE for systems of water + nine cholinium-based ILs by means of a humidity meter instrument. COSMO-RS model was used to correlate the experimental data and to show the interaction of water and the type of anion of the IL. They concluded that water presented the strongest interaction with [Cho][OAc] due to the lowest activity coefficient.
In this work we carried out a comprehensive experimental study of the water sorption equilibrium on [Cho][OAc], which is particularly promising for the use of thermally-driven sorption technologies. Water

sorption equilibrium was measured using a gravimetric dynamic vapour sorption apparatus at different temperatures from 298.25 to 349.55 K. Then, we correlated the experimental data with two models that are typical of adsorption equilibria, namely the Guggenheim-Anderson-de Boer (GAB) model, and the VL equilibria, namely the Redlich-Kister (RK) excess Gibbs energy model. After successful regression of the parameters, we also showed how to predict molar excess properties using the RK model including Gibbs energy, enthalpy and entropy. It is crucial to know the thermophysical properties of the IL, especially its melting point when it is integrated in a heat transformer. [Cho][OAc] is a solid at room temperature and has a wide range of reported melting points in the literature, as shown in Table 1. Finally, a thermodynamic cycle analysis that uses the experimental isotherm data was assessed to evaluate the suitability of the material for sorption chillers through the coefficient of performance (COP).

Table 1: Melting and degradation temperature data for [Cho][OAc] ionic liquid.

Melting temperature [°C]	Degradation temperature [°C]	Reference
51	190	Colomines et al. [24]
51	189	Fukaya et al. [25]
63.4	-	Cheng et al. [26]
67.6	-	Lopes et al. [27]
72	-	Muhammad et al. [28]
80	-	Zhang et al. [29]
89.4	-	Fernandez et al. [30]

2. Experimental

2.1 Materials

2-hydroxyethyl-trimethylammonium acetate ionic liquid [Cho][OAc] ≥ 95.0% was supplied by Sigma-Aldrich where water was present as an impurity ≤ 1% [31]. The material was stored in an airtight bottle at room temperature away from direct sun light to ensure nothing affected the quality of the product. All samples were used without any further purification.

2.2 Apparatus and procedure

Water sorption equilibrium was measured using a gravimetric dynamic vapour sorption system (DVS) from Surface Measurement Systems [32] that provides a fast and accurate method for analysis. The apparatus schematic is shown in Figure 1.

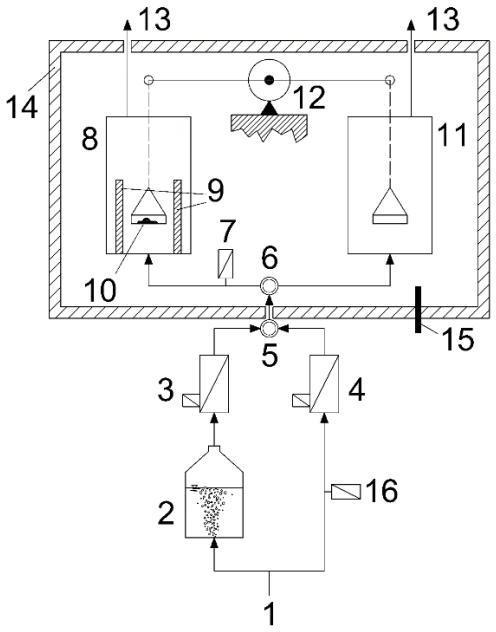

Figure 1: Schematic of DVS system used for the measurement of water sorption equilibrium data. 1. Nitrogen inlet; 2. Water bubbler; 3. Wet nitrogen stream mass flow controller; 4. Dry nitrogen stream mass flow controller; 5. Mixing tee; 6. Splitter tee; 7. Humidity and sorption temperature sensor; 8. Sample cell; 9. Electric heater; 10. Sample; 11. Reference cell; 12. Microbalance; 13. System outlets; 14. Insulated and thermostated air enclosure; 15. Incubator temperature sensor; 16. Dry nitrogen humidity sensor.

Two pans hang from wires connected to a microbalance, one holds the sample and the other is used as a reference weight. The symmetric microbalance scale minimizes buoyancy effects. For the equilibrium measurements, pure nitrogen gas and water vapour flow through the system at a constant flowrate. The microbalance weighs the sample with a 0.1 μg stable resolution. The temperature of the incubator is measured by a platinum resistance thermometer (PT100 sensor). Relative humidity (RH) and temperature measurements of the nitrogen/water vapour mixture are performed with an HC2A Humidity Temperature Probe (Rotronic) while two MFC 2000 (Axetris) high accuracy digital mass flow controllers control the flow of water vapour and nitrogen into the system. The apparatus can be used for water sorption measurements for temperatures between 5 and 85°C and RH up to 98%. Humidity and temperature probes are located close to the sample pan. The equilibrium water uptake of the sample was calculated from the mass of the sample at each equilibrium value with the following relation:

$$W = \frac{m - m_0}{m_0} \tag{1}$$

where W is the uptake of water into [Cho][OAc] expressed in $g_W\ g_{IL}^{-1}$, m_o is the bone-dry weight of the sample expressed in mg, and m is the mass of the sample at equilibrium expressed in mg.
Temperature inside the DVS system remains constant at a set value throughout the entire cycle, allowing the user to examine water sorption measurements over a wide range. A total of eight temperatures (298.25, 303.25, 308.35, 318.55, 328.75, 333.85, 344.15 and 349.55 K) were examined. Samples were loaded into the sample cell and let reach the specified equilibrium temperature and a stable weight all the time under a 200 SCCM of dry nitrogen flow per mass flow controller. Once at equilibrium, the [Cho][OAc] samples were first regenerated at 90°C for 8 hours under dry nitrogen flow to desorb all water. After that, the samples were stabilized at the sorption temperature still under dry nitrogen flow for 2 hours, at which point they were considered dry and ready for the sorption measurements.
Sorption isotherms were measured under a constant flow of nitrogen gas at 200 SCCM for gradual steps from 0% to 98% of RH. The conditions inside the chamber were held at constant temperature and RH until the mass of the sample reached equilibrium. Equilibrium was determined when the mass change (dm/dt) equaled 0.002% min^{-1} or 20 μg g^{-1} min^{-1} over a 10-minute period, following the approach used by Glass et al. [33].

2.3 Uncertainty analysis

The humidity and temperature probe has a uncertainty on relative humidity (σ_{RH}) of ±0.8% at 10−30°C, ±1.3% at 30−60°C, ±1.8% at 60−100°C and temperature uncertainty (σ_T) of ±0.1 K. A blank experiment was carried out in order to attain the weighing uncertainty of the instrument. The results showed a sample mass uncertainty (σ_m, $\sigma_{m0,w}$) of $\pm 5.0 \cdot 10^{-4}$ mg. When the measurement values are manipulated by calculations such as converting the mass of the water sorbed into water uptake or calculating water mole fractions and activity coefficients, the following set of equations was applied to determine the error propagation on the standard deviations:

$$R = X + Y - Z \tag{2}$$

$$\sigma_R = \sqrt{\sigma_X^2 + \sigma_Y^2 + \sigma_Z^2} \tag{3}$$

$$R' = \frac{X' \cdot Y'}{Z'} \tag{4}$$

$$\sigma_{R'} = |R'| \cdot \sqrt{\left(\frac{\sigma_{X'}}{X'}\right)^2 + \left(\frac{\sigma_{Y'}}{Y'}\right)^2 + \left(\frac{\sigma_{Z'}}{Z'}\right)^2} \tag{5}$$

where X, Y, Z, X', Y', Z' are measured variables, R, R' are calculated variables and σ refer to the uncertainties of the calculated variables.
In addition to Eq. (1) that was used to calculate the water uptake from the sample mass, the additional Eqns (6−7) were employed to calculate water mole fractions and activity coefficients:

$$x_W = \frac{W}{W + \frac{MW_W}{MW_{IL}}} \tag{6}$$

$$\gamma_W = \frac{P}{P_W^S \cdot x_W} = \frac{RH}{100 \cdot x_W} \tag{7}$$

where x_W is the mole fraction of water in the IL-rich phase, MW_W is the molecular weight of water (18.0 g mol^{-1}), MW_{IL} is the molecular weight of [Cho][OAc] (163.2 g mol^{-1}), γ_W is the activity coefficient of water in the IL-rich phase, P is the pressure of water in the vapour phase and P^S_W is the saturation pressure of water at the equilibrium temperature. Note that the ratio (P/P^S_W) corresponds to the relative humidity (RH) and the uncertainty of the water partial pressure is the same of the relative humidity. In addition, the uncertainty on the water content of the samples at the beginning of the experiments ($\sigma_{m0,RH}$) was estimated from the uncertainty at ambient temperature on the dry nitrogen humidity sensor of ±0.8% and resulted in 0.12% of the bone-dry weight of the sample. The overall uncertainty on the initial sample mass (σ_{m0}) combines the uncertainty of the dry nitrogen relative humidity and the weighing uncertainty of the instrument by taking the square root of the sum of their squares, as reported in Eq. (8):

$$\sigma_{m0} = \sqrt{\sigma^2_{m0,RH} + \sigma^2_{m0,w}} \tag{8}$$

Applying the above Eqns (2−5) the uncertainties of the calculated variables were evaluated as follows:

$$\sigma_W = |W| \cdot \sqrt{\left(\frac{\sqrt{\sigma_m^2+\sigma_{m0}^2}}{m-m_0}\right)^2 + \left(\frac{\sigma_{m0}}{m_0}\right)^2} \tag{9}$$

$$\sigma_x = |x_W| \cdot \sqrt{2 \cdot \left(\frac{\sigma_W}{W}\right)^2} \tag{10}$$

$$\sigma_\gamma = |\gamma_W| \cdot \sqrt{\left(\frac{\sigma_{RH}}{RH}\right)^2 + \left(\frac{\sigma_x}{x_W}\right)^2} \tag{11}$$

3 Results and discussion

3.1 Experimental results

The water sorption equilibrium data on [Cho][OAc] are listed in Tables 2−9 for 298.25, 303.25, 308.35, 318.55, 328.75, 333.85, 344.15 and 349.55 K, respectively. The reported variables are relative humidity, water partial pressure, water uptake, water mole fraction, water activity coefficient and the associated uncertainties. The whole analysis assumes the solubility of nitrogen in the ionic liquid as negligible.

Table 2: Experimental water sorption equilibrium data on [Cho][OAc] at 298.25 K with m_0 = 6.447 mg.

RH [%]	P [kPa]	W [g_W g_{IL}^{-1}]	x_W [-]	γ_W [-]	σ_W [g_W g_{IL}^{-1}]	σ_x [-]	σ_γ [-]
48.630	1.551	0.667	0.858	0.567	$1.45\cdot10^{-3}$	$2.63\cdot10^{-3}$	$9.48\cdot10^{-3}$
48.690	1.553	0.670	0.859	0.567	$1.45\cdot10^{-3}$	$2.63\cdot10^{-3}$	$9.48\cdot10^{-3}$
77.010	2.457	1.421	0.928	0.830	$2.09\cdot10^{-3}$	$1.93\cdot10^{-3}$	$8.79\cdot10^{-3}$
77.185	2.462	1.433	0.929	0.831	$2.10\cdot10^{-3}$	$1.93\cdot10^{-3}$	$8.79\cdot10^{-3}$
85.495	2.727	2.148	0.951	0.899	$2.85\cdot10^{-3}$	$1.78\cdot10^{-3}$	$8.58\cdot10^{-3}$
85.530	2.728	2.168	0.952	0.899	$2.87\cdot10^{-3}$	$1.78\cdot10^{-3}$	$8.57\cdot10^{-3}$
86.870	2.771	2.410	0.956	0.908	$3.14\cdot10^{-3}$	$1.76\cdot10^{-3}$	$8.53\cdot10^{-3}$
87.085	2.778	2.378	0.956	0.911	$3.10\cdot10^{-3}$	$1.76\cdot10^{-3}$	$8.54\cdot10^{-3}$
89.115	2.843	2.807	0.962	0.926	$3.58\cdot10^{-3}$	$1.74\cdot10^{-3}$	$8.48\cdot10^{-3}$
89.255	2.847	2.961	0.964	0.926	$3.76\cdot10^{-3}$	$1.73\cdot10^{-3}$	$8.46\cdot10^{-3}$
90.610	2.890	3.215	0.967	0.937	$4.05\cdot10^{-3}$	$1.72\cdot10^{-3}$	$8.44\cdot10^{-3}$
91.510	2.919	3.525	0.970	0.944	$4.41\cdot10^{-3}$	$1.71\cdot10^{-3}$	$8.42\cdot10^{-3}$

Table 3: Experimental water sorption equilibrium data on [Cho][OAc] at 303.25 K with m_0 = 7.676 mg.

RH [%]	P [kPa]	W [g_W g_{IL}^{-1}]	x_W [-]	γ_W [-]	σ_W [g_W g_{IL}^{-1}]	σ_x [-]	σ_γ [-]
49.780	2.127	0.682	0.861	0.578	$1.46\cdot10^{-3}$	$2.60\cdot10^{-3}$	$9.46\cdot10^{-3}$
76.880	3.284	1.439	0.929	0.828	$2.11\cdot10^{-3}$	$1.92\cdot10^{-3}$	$8.78\cdot10^{-3}$
85.560	3.655	2.238	0.953	0.898	$2.95\cdot10^{-3}$	$1.77\cdot10^{-3}$	$8.56\cdot10^{-3}$

87.200	3.725	2.550	0.959	0.910	$3.29 \cdot 10^{-3}$	$1.75 \cdot 10^{-3}$	$8.51 \cdot 10^{-3}$
89.840	3.838	3.156	0.966	0.930	$3.98 \cdot 10^{-3}$	$1.72 \cdot 10^{-3}$	$8.44 \cdot 10^{-3}$
91.315	3.901	3.766	0.972	0.940	$4.68 \cdot 10^{-3}$	$1.71 \cdot 10^{-3}$	$8.40 \cdot 10^{-3}$

Table 4: Experimental water sorption equilibrium data on [Cho][OAc] at 308.35 K with m_0 = 7.638 mg.

RH [%]	P [kPa]	W [$g_W\ g_{IL}^{-1}$]	x_W [-]	γ_W [-]	σ_W [$g_W\ g_{IL}^{-1}$]	σ_x [-]	σ_γ [-]
15.105	0.860	0.267	0.707	0.214	$1.25 \cdot 10^{-3}$	$4.67 \cdot 10^{-3}$	$1.84 \cdot 10^{-2}$
30.065	1.711	0.427	0.795	0.378	$1.31 \cdot 10^{-3}$	$3.45 \cdot 10^{-3}$	$1.64 \cdot 10^{-2}$
49.190	2.800	0.670	0.859	0.573	$1.45 \cdot 10^{-3}$	$2.62 \cdot 10^{-3}$	$1.52 \cdot 10^{-2}$
66.885	3.807	1.041	0.904	0.740	$1.74 \cdot 10^{-3}$	$2.13 \cdot 10^{-3}$	$1.45 \cdot 10^{-2}$
75.840	4.317	1.405	0.927	0.818	$2.07 \cdot 10^{-3}$	$1.94 \cdot 10^{-3}$	$1.41 \cdot 10^{-2}$
80.590	4.587	1.714	0.940	0.858	$2.39 \cdot 10^{-3}$	$1.85 \cdot 10^{-3}$	$1.39 \cdot 10^{-2}$
85.075	4.842	2.238	0.953	0.893	$2.95 \cdot 10^{-3}$	$1.77 \cdot 10^{-3}$	$1.37 \cdot 10^{-2}$
89.690	5.105	3.164	0.966	0.928	$3.99 \cdot 10^{-3}$	$1.72 \cdot 10^{-3}$	$1.36 \cdot 10^{-2}$

Table 5: Experimental water sorption equilibrium data on [Cho][OAc] at 318.55 K with m_0 = 8.626 mg.

RH [%]	P [kPa]	W [$g_W\ g_{IL}^{-1}$]	x_W [-]	γ_W [-]	σ_W [$g_W\ g_{IL}^{-1}$]	σ_x [-]	σ_γ [-]
15.205	1.489	0.258	0.700	0.217	$1.24 \cdot 10^{-3}$	$4.77 \cdot 10^{-3}$	$1.86 \cdot 10^{-2}$
15.580	1.526	0.265	0.706	0.221	$1.24 \cdot 10^{-3}$	$4.69 \cdot 10^{-3}$	$1.85 \cdot 10^{-2}$
30.075	2.946	0.417	0.791	0.380	$1.30 \cdot 10^{-3}$	$3.50 \cdot 10^{-3}$	$1.65 \cdot 10^{-2}$
31.220	3.058	0.433	0.797	0.392	$1.31 \cdot 10^{-3}$	$3.41 \cdot 10^{-3}$	$1.64 \cdot 10^{-2}$
48.675	4.767	0.656	0.856	0.569	$1.44 \cdot 10^{-3}$	$2.65 \cdot 10^{-3}$	$1.53 \cdot 10^{-2}$
50.840	4.979	0.696	0.863	0.589	$1.46 \cdot 10^{-3}$	$2.57 \cdot 10^{-3}$	$1.52 \cdot 10^{-2}$
65.360	6.401	1.009	0.901	0.725	$1.71 \cdot 10^{-3}$	$2.16 \cdot 10^{-3}$	$1.45 \cdot 10^{-2}$
65.620	6.427	1.024	0.903	0.727	$1.72 \cdot 10^{-3}$	$2.15 \cdot 10^{-3}$	$1.45 \cdot 10^{-2}$
74.810	7.327	1.362	0.925	0.809	$2.03 \cdot 10^{-3}$	$1.95 \cdot 10^{-3}$	$1.42 \cdot 10^{-2}$
74.940	7.340	1.387	0.926	0.809	$2.05 \cdot 10^{-3}$	$1.94 \cdot 10^{-3}$	$1.41 \cdot 10^{-2}$
79.670	7.803	1.719	0.940	0.848	$2.39 \cdot 10^{-3}$	$1.85 \cdot 10^{-3}$	$1.39 \cdot 10^{-2}$
79.735	7.809	1.679	0.938	0.850	$2.35 \cdot 10^{-3}$	$1.86 \cdot 10^{-3}$	$1.40 \cdot 10^{-2}$
84.460	8.272	2.262	0.953	0.886	$2.97 \cdot 10^{-3}$	$1.77 \cdot 10^{-3}$	$1.37 \cdot 10^{-2}$
84.480	8.274	2.286	0.954	0.886	$3.00 \cdot 10^{-3}$	$1.77 \cdot 10^{-3}$	$1.37 \cdot 10^{-2}$
89.185	8.735	3.354	0.968	0.921	$4.21 \cdot 10^{-3}$	$1.72 \cdot 10^{-3}$	$1.35 \cdot 10^{-2}$
89.265	8.743	3.652	0.971	0.920	$4.55 \cdot 10^{-3}$	$1.71 \cdot 10^{-3}$	$1.35 \cdot 10^{-2}$

Table 6: Experimental water sorption equilibrium data on [Cho][OAc] at 328.75 K with m_0 = 6.091 mg.

RH [%]	P [kPa]	W [$g_W\ g_{IL}^{-1}$]	x_W [-]	γ_W [-]	σ_W [$g_W\ g_{IL}^{-1}$]	σ_x [-]	σ_γ [-]
15.925	2.583	0.261	0.703	0.226	$1.25 \cdot 10^{-3}$	$4.74 \cdot 10^{-3}$	$1.86 \cdot 10^{-2}$
16.100	2.611	0.259	0.702	0.229	$1.25 \cdot 10^{-3}$	$4.77 \cdot 10^{-3}$	$1.86 \cdot 10^{-2}$
30.820	4.999	0.428	0.795	0.388	$1.31 \cdot 10^{-3}$	$3.44 \cdot 10^{-3}$	$1.64 \cdot 10^{-2}$
30.930	5.017	0.423	0.793	0.390	$1.31 \cdot 10^{-3}$	$3.47 \cdot 10^{-3}$	$1.65 \cdot 10^{-2}$
49.235	7.986	0.668	0.858	0.574	$1.45 \cdot 10^{-3}$	$2.63 \cdot 10^{-3}$	$1.52 \cdot 10^{-2}$
49.290	7.995	0.677	0.860	0.573	$1.46 \cdot 10^{-3}$	$2.61 \cdot 10^{-3}$	$1.52 \cdot 10^{-2}$
64.320	10.433	0.999	0.901	0.714	$1.70 \cdot 10^{-3}$	$2.17 \cdot 10^{-3}$	$1.45 \cdot 10^{-2}$
64.465	10.456	1.023	0.903	0.714	$1.72 \cdot 10^{-3}$	$2.15 \cdot 10^{-3}$	$1.45 \cdot 10^{-2}$
73.020	11.844	1.341	0.924	0.790	$2.01 \cdot 10^{-3}$	$1.96 \cdot 10^{-3}$	$1.42 \cdot 10^{-2}$
73.395	11.905	1.378	0.926	0.793	$2.05 \cdot 10^{-3}$	$1.95 \cdot 10^{-3}$	$1.41 \cdot 10^{-2}$
77.935	12.641	1.662	0.938	0.831	$2.33 \cdot 10^{-3}$	$1.86 \cdot 10^{-3}$	$1.40 \cdot 10^{-2}$
82.750	13.422	2.175	0.952	0.869	$2.88 \cdot 10^{-3}$	$1.78 \cdot 10^{-3}$	$1.38 \cdot 10^{-2}$
83.415	13.530	2.325	0.955	0.874	$3.05 \cdot 10^{-3}$	$1.77 \cdot 10^{-3}$	$1.37 \cdot 10^{-2}$

87.625	14.213	3.434	0.969	0.904	$4.30 \cdot 10^{-3}$	$1.72 \cdot 10^{-3}$	$1.35 \cdot 10^{-2}$
87.990	14.272	3.531	0.970	0.907	$4.41 \cdot 10^{-3}$	$1.71 \cdot 10^{-3}$	$1.35 \cdot 10^{-2}$
88.400	14.338	3.762	0.972	0.910	$4.68 \cdot 10^{-3}$	$1.71 \cdot 10^{-3}$	$1.35 \cdot 10^{-2}$

Table 7: Experimental water sorption equilibrium data on [Cho][OAc] at 333.85 K with m_0 = 7.587 mg.

RH [%]	P [kPa]	W [$g_W\ g_{IL}^{-1}$]	x_W [-]	γ_W [-]	σ_W [$g_W\ g_{IL}^{-1}$]	σ_x [-]	σ_γ [-]
16.430	3.385	0.250	0.694	0.237	$1.24 \cdot 10^{-3}$	$4.86 \cdot 10^{-3}$	$1.88 \cdot 10^{-2}$
16.670	3.434	0.255	0.698	0.239	$1.24 \cdot 10^{-3}$	$4.81 \cdot 10^{-3}$	$1.87 \cdot 10^{-2}$
31.070	6.401	0.415	0.790	0.393	$1.30 \cdot 10^{-3}$	$3.51 \cdot 10^{-3}$	$1.65 \cdot 10^{-2}$
31.405	6.470	0.422	0.793	0.396	$1.31 \cdot 10^{-3}$	$3.47 \cdot 10^{-3}$	$1.65 \cdot 10^{-2}$
49.780	10.255	0.669	0.858	0.580	$1.45 \cdot 10^{-3}$	$2.63 \cdot 10^{-3}$	$1.52 \cdot 10^{-2}$
48.980	10.090	0.654	0.856	0.572	$1.44 \cdot 10^{-3}$	$2.66 \cdot 10^{-3}$	$1.53 \cdot 10^{-2}$
63.050	12.989	0.957	0.897	0.703	$1.66 \cdot 10^{-3}$	$2.21 \cdot 10^{-3}$	$1.46 \cdot 10^{-2}$
64.225	13.231	0.992	0.900	0.714	$1.69 \cdot 10^{-3}$	$2.17 \cdot 10^{-3}$	$1.45 \cdot 10^{-2}$
71.410	14.711	1.266	0.920	0.776	$1.94 \cdot 10^{-3}$	$1.99 \cdot 10^{-3}$	$1.42 \cdot 10^{-2}$
72.680	14.973	1.326	0.923	0.787	$2.00 \cdot 10^{-3}$	$1.97 \cdot 10^{-3}$	$1.42 \cdot 10^{-2}$
76.510	15.762	1.565	0.934	0.819	$2.23 \cdot 10^{-3}$	$1.89 \cdot 10^{-3}$	$1.40 \cdot 10^{-2}$
77.250	15.914	1.621	0.936	0.825	$2.29 \cdot 10^{-3}$	$1.87 \cdot 10^{-3}$	$1.40 \cdot 10^{-2}$
81.655	16.822	2.032	0.949	0.861	$2.72 \cdot 10^{-3}$	$1.80 \cdot 10^{-3}$	$1.38 \cdot 10^{-2}$
81.920	16.876	2.101	0.950	0.862	$2.80 \cdot 10^{-3}$	$1.79 \cdot 10^{-3}$	$1.38 \cdot 10^{-2}$
86.120	17.742	2.984	0.964	0.893	$3.78 \cdot 10^{-3}$	$1.73 \cdot 10^{-3}$	$1.36 \cdot 10^{-2}$
86.200	17.758	2.984	0.964	0.894	$3.78 \cdot 10^{-3}$	$1.73 \cdot 10^{-3}$	$1.36 \cdot 10^{-2}$

Table 8: Experimental water sorption equilibrium data on [Cho][OAc] at 344.15 K with m_0 = 4.737 mg.

RH [%]	P [kPa]	W [$g_W\ g_{IL}^{-1}$]	x_W [-]	γ_W [-]	σ_W [$g_W\ g_{IL}^{-1}$]	σ_x [-]	σ_γ [-]
33.615	10.950	0.431	0.796	0.422	$1.32 \cdot 10^{-3}$	$3.44 \cdot 10^{-3}$	$2.27 \cdot 10^{-2}$
50.575	16.475	0.663	0.857	0.590	$1.45 \cdot 10^{-3}$	$2.65 \cdot 10^{-3}$	$2.11 \cdot 10^{-2}$
62.355	20.313	0.920	0.893	0.698	$1.64 \cdot 10^{-3}$	$2.25 \cdot 10^{-3}$	$2.02 \cdot 10^{-2}$
68.800	22.412	1.140	0.912	0.755	$1.83 \cdot 10^{-3}$	$2.07 \cdot 10^{-3}$	$1.98 \cdot 10^{-2}$
70.060	22.823	1.199	0.916	0.765	$1.88 \cdot 10^{-3}$	$2.03 \cdot 10^{-3}$	$1.97 \cdot 10^{-2}$
71.780	23.383	1.271	0.920	0.780	$1.95 \cdot 10^{-3}$	$2.00 \cdot 10^{-3}$	$1.96 \cdot 10^{-2}$
73.120	23.820	1.350	0.924	0.791	$2.03 \cdot 10^{-3}$	$1.96 \cdot 10^{-3}$	$1.95 \cdot 10^{-2}$
75.405	24.564	1.463	0.930	0.811	$2.14 \cdot 10^{-3}$	$1.92 \cdot 10^{-3}$	$1.94 \cdot 10^{-2}$
80.350	26.175	1.908	0.945	0.850	$2.60 \cdot 10^{-3}$	$1.82 \cdot 10^{-3}$	$1.91 \cdot 10^{-2}$
81.585	26.577	2.054	0.949	0.860	$2.75 \cdot 10^{-3}$	$1.80 \cdot 10^{-3}$	$1.90 \cdot 10^{-2}$
82.105	26.747	2.154	0.951	0.863	$2.86 \cdot 10^{-3}$	$1.79 \cdot 10^{-3}$	$1.90 \cdot 10^{-2}$

Table 9: Experimental water sorption equilibrium data on [Cho][OAc] at 349.55 K with m_0 = 11.019 mg.

RH [%]	P [kPa]	W [$g_W\ g_{IL}^{-1}$]	x_W [-]	γ_W [-]	σ_W [$g_W\ g_{IL}^{-1}$]	σ_x [-]	σ_γ [-]
18.815	7.698	0.267	0.708	0.266	$1.24 \cdot 10^{-3}$	$4.66 \cdot 10^{-3}$	$2.55 \cdot 10^{-2}$
19.295	7.894	0.271	0.711	0.271	$1.25 \cdot 10^{-3}$	$4.62 \cdot 10^{-3}$	$2.54 \cdot 10^{-2}$
33.665	13.774	0.427	0.795	0.424	$1.31 \cdot 10^{-3}$	$3.44 \cdot 10^{-3}$	$2.27 \cdot 10^{-2}$
34.815	14.244	0.437	0.799	0.436	$1.31 \cdot 10^{-3}$	$3.39 \cdot 10^{-3}$	$2.26 \cdot 10^{-2}$
48.555	19.866	0.639	0.853	0.569	$1.43 \cdot 10^{-3}$	$2.69 \cdot 10^{-3}$	$2.12 \cdot 10^{-2}$
49.870	20.404	0.657	0.856	0.582	$1.44 \cdot 10^{-3}$	$2.65 \cdot 10^{-3}$	$2.11 \cdot 10^{-2}$
59.250	24.242	0.855	0.886	0.669	$1.58 \cdot 10^{-3}$	$2.32 \cdot 10^{-3}$	$2.04 \cdot 10^{-2}$
60.305	24.673	0.884	0.889	0.678	$1.60 \cdot 10^{-3}$	$2.28 \cdot 10^{-3}$	$2.03 \cdot 10^{-2}$
66.080	27.036	1.057	0.906	0.730	$1.75 \cdot 10^{-3}$	$2.12 \cdot 10^{-3}$	$2.00 \cdot 10^{-2}$
66.330	27.138	1.082	0.908	0.731	$1.77 \cdot 10^{-3}$	$2.10 \cdot 10^{-3}$	$1.99 \cdot 10^{-2}$

73.210	29.953	1.400	0.927	0.790	$2.07 \cdot 10^{-3}$	$1.93 \cdot 10^{-3}$	$1.95 \cdot 10^{-2}$

Figures 2 and 3 show the water adsorption isotherms on [Cho][OAc] as water uptake against relative humidity at two temperature levels: low temperatures comprising 298.25, 303.25, 308.35 and 318.55 K and high temperatures comprising 328.75, 333.85, 344.15 and 349.55 K. Water isotherms on [Cho][OAc] at 298.15 K from [23] and on [EMIM][OAc] at 303.15 K from [20] were also reported in the same figures as references. As expected, [Cho][OAc] followed the same trend of other ILs, showing a type III isotherm for water at all temperatures. In the whole RH range it can be observed that at constant relative humidity the maximum difference in water uptake across the isotherms was 0.25 $g_W\ g_{IL}^{-1}$. With a relative humidity of around 90% an exceptional water uptake larger than 3.5 $g_W\ g_{IL}^{-1}$ was observed for all the temperatures.

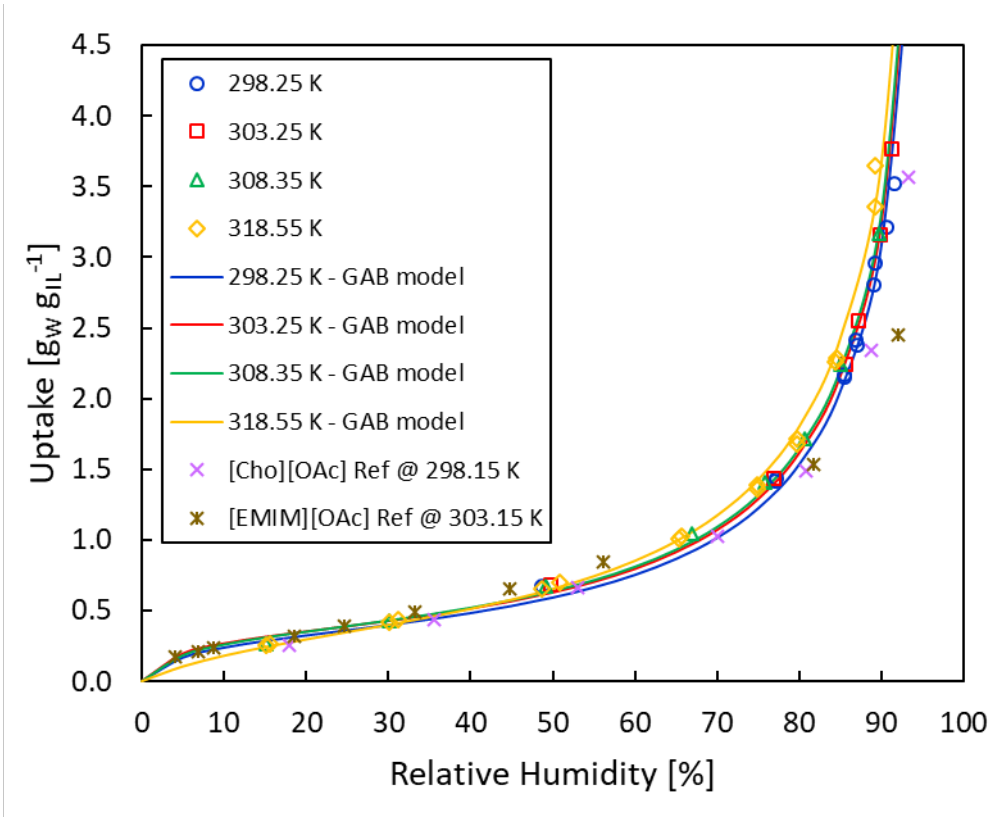

Figure 2: Water sorption isotherms on [Cho][OAc] at low temperatures: 298.25, 303.25, 308.35 and 318.55 K. Reference [Cho][OAc] from [23] is at 298.15 K and reference [EMIM][OAc] from [20] is at 303.15 K. GAB model parameters are reported in Table 10.

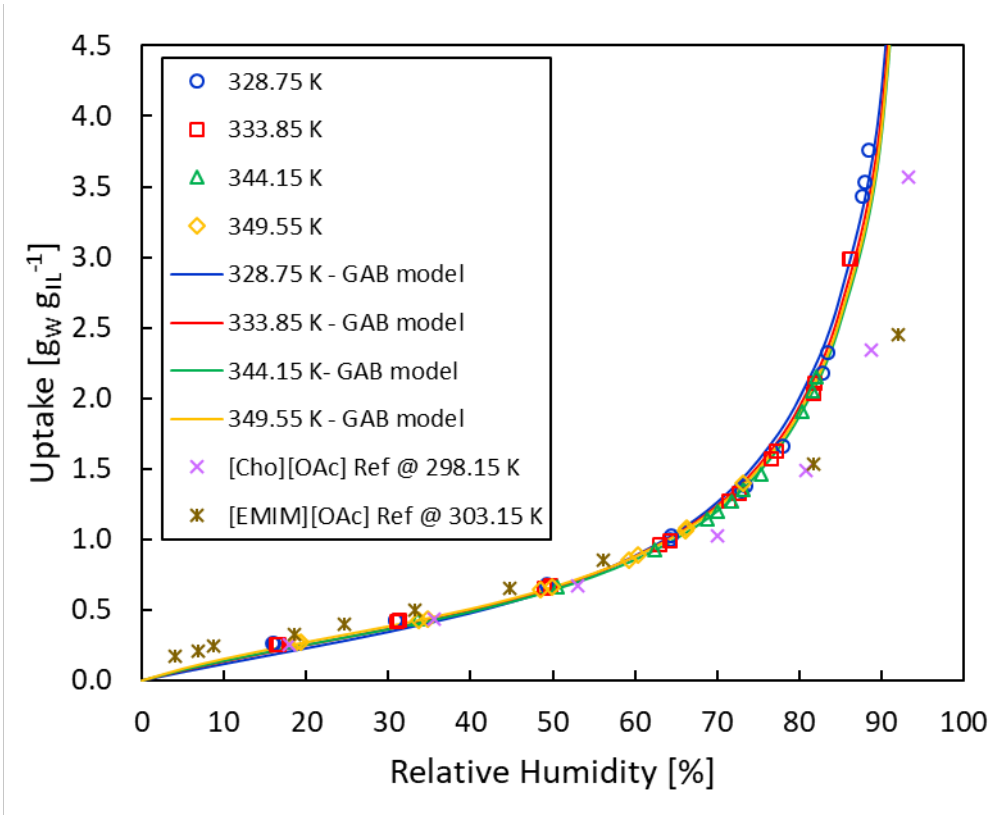

Figure 3: Water sorption isotherms on [Cho][OAc] at high temperatures: 328.75, 333.85, 344.15 and 349.55 K. Reference [Cho][OAc] from [23] is at 298.15 K and reference [EMIM][OAc] from [20] is at 303.15 K. GAB model parameters are reported in Table 10.

The measured experimental data at 298.25 K matched well with the reference data at the same temperature. It is worth noticing the difference between the uptake of water on [Cho][OAc] and [EMIM][OAc] at nearly ambient temperature. Both ILs share the same acetate anion but water uptake in [Cho][OAc] is higher at high relative humidity likely because of the hydroxyl group in the choline cation.

While the water uptake increases from 349.55 to 328.75 K it then sharply decreases at 318.55 K and increases again up to 298.25 K. This can be explained by the crossing of [Cho][OAc] melting point. At temperatures of 328.75 K and above, the [Cho][OAc] is a liquid and absorption measurements are gathered. When the temperature is lowered to 318.55 K, in presence of water [Cho][OAc] can in part crystallize in a solid and in part supercool as a liquid. When the temperature is 308.35 K and below, the presence of a single characteristic curve suggests that the system is composed by one single phase. The phase transition is, in fact, confirmed by analysing the Gibbs energy difference between the absorbed state and the water saturation state ($\Delta g = -RTln(P/P^S_W) = -RTln(RH)$), which results in a temperature-independent curve characteristic of the particular sorbent/sorbate [8,34]. Figure 4 shows the water uptake versus Δg on [Cho][OAc] for all the temperatures investigated. There exist two distinct characteristic curves at low temperatures (open symbols) and high temperatures (full symbols) that eventually overlap in low water uptake region. The two curves denote the different states of [Cho][OAc] which is a solid or liquid depending on the combination of temperature and relative humidity.

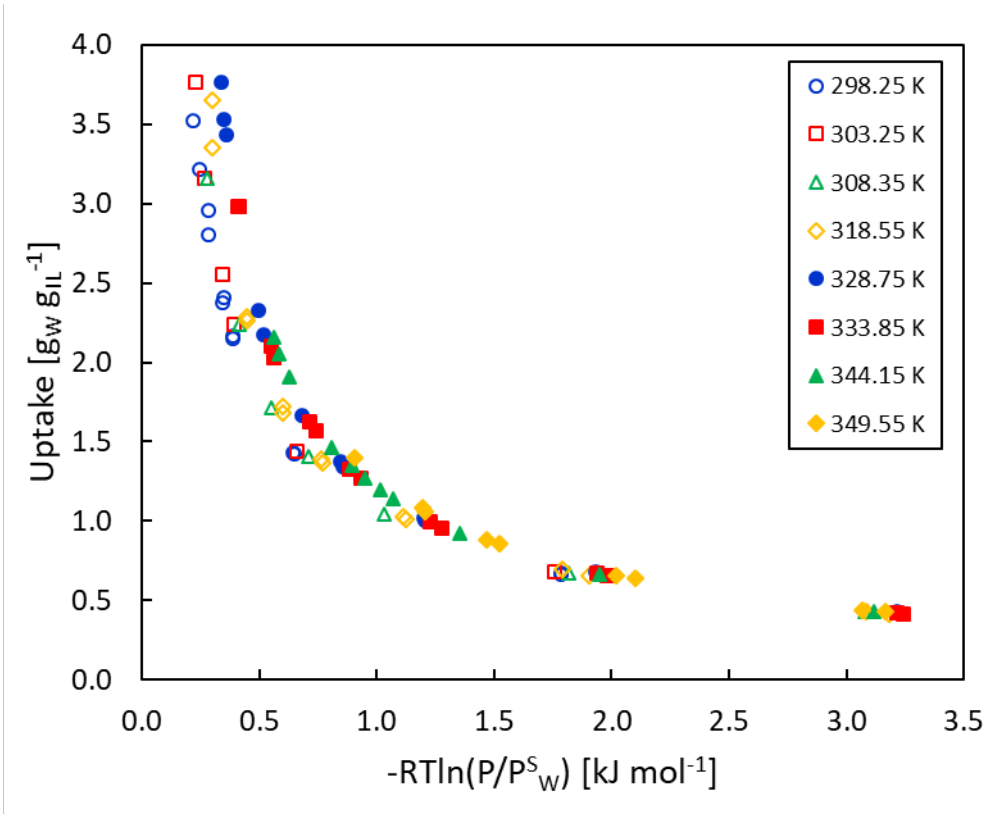

Figure 4: Characteristic curves of water sorption on [Cho][OAc] at different temperatures. Data at low temperatures (open symbols) denoting a solid state for [Cho][OAc] collapse on a lower single temperature-independent curve. Data at high temperatures (full symbols) denoting a liquid state for [Cho][OAc] collapse on a higher single temperature-independent curve.

3.2 Sorption equilibrium with the Guggenheim-Anderson-de Boer model

Given the phase transition of [Cho][OAc] in the investigated range of temperatures the first modelling approach was related to adsorption equilibria. The experimental data were correlated using the Guggenheim-Anderson-de Boer model which was proven to accurately describe type III isotherms [35]. The GAB model can be expressed as:

$$W = W_m \cdot \frac{C \cdot K \cdot \left(\frac{P}{P^S}\right)}{\left(1 - K \cdot \left(\frac{P}{P^S}\right)\right) \cdot \left(1 - K \cdot \left(\frac{P}{P^S}\right) + C \cdot K \cdot \left(\frac{P}{P^S}\right)\right)} \tag{12}$$

where W_m is the water uptake corresponding to monolayer saturation expressed in $g_W\ g_{IL}^{-1}$, C is the Guggenheim constant and K is a correction factor of the monolayer adsorption. Assuming pure monolayer adsorption for which $K=1$ the GAB parameters W_m and C were calculated by minimizing the following objective function:

$$OF = \sum_{i=1}^{n} \left(\frac{W_{calc,i} - W_{exp,i}}{W_{exp,i}}\right)^2 \tag{13}$$

The regressed parameters along with the coefficients of determination (R^2) are reported in Table 10. Figures 2 and 3 show an excellent agreement between the experimental data and the fit using the GAB model, also corroborated by the R^2 values being very close to 1.

Table 10: Parameters of GAB model and coefficients of determination for water sorption on [Cho][OAc] at different temperatures.

T [K]	W_m [$g_W\ g_{IL}^{-1}$]	C [-]	K [-]	R^2
298.25	0.311	19.901	1.000	0.993
303.25	0.327	25.050	1.000	0.999

308.35	0.334	20.877	1.000	0.998
318.55	0.374	6.918	1.000	0.995
328.75	0.435	2.917	1.000	0.993
333.85	0.414	3.808	1.000	0.995
344.15	0.398	4.195	1.000	0.998
349.55	0.401	4.799	1.000	1.000

Note: The isotherm coefficients of this table can be replaced by an Arrhenius-type temperature-dependent expression for $C = C_0 \exp\left(-\frac{E_a}{R \cdot T}\right)$, resulting in the following set of parameters: $W_m = 0.427 g_W \, g_{IL}^{-1}$, $C_0 = 4.56$, $E_a = 49.9 \, J \, mol^{-1}$, $K = 0.97$

The GAB model was further fitted with only four parameters valid in the entire temperature range from 298.25 K to 349.55 K. The coefficient C was replaced by an Arrhenius-type temperature-dependent relation $C = C_0 \exp\left(-\frac{E_a}{R \cdot T}\right)$. The following regressed parameters were obtained: $W_m = 0.427 g_W \, g_{IL}^{-1}$, $C_0 = 4.56$, $E_a = 49.9 \, J \, mol^{-1}$ and $K = 0.97$.

3.3 Sorption equilibrium with the Redlich-Kister excess Gibbs energy model

The second modelling approach, typical of VL equilibria, was related to excess Gibbs energy models capable to describe the thermodynamic behavior of ILs between confined and non-confined states. It was reported that NRTL and UNIQUAC models can accurately predict several water/IL systems [21,22]. However, as demonstrated by Askalany et al. [8], the simpler three-parameter Redlich-Kister excess Gibbs energy model can correlate many VLE systems with low errors. The molar Gibbs energy difference between the confined state and pure water at saturation can be expressed as the sum of the ideal mixture contribution and the excess mixture contribution, defined as follows:

$$\Delta g = \Delta g^{ID} + \Delta g^{EX} \quad (14)$$

with

$$\Delta g^{ID} = R \cdot T \cdot ln(x_W) \quad (15)$$

and

$$\Delta g^{EX} = R \cdot T \cdot x_W \cdot (1 - x_W) \cdot [A + B \cdot (2 \cdot x_W - 1) + C \cdot (2 \cdot x_W - 1)^2] \quad (16)$$

where A, B and C are the model parameters and x_W can be converted in water uptake (W) using Eq. (6). Regressed parameters were obtained with a similar procedure described in paragraph 3.2 for the GAB model. Table 11 lists the RK parameters with the respective coefficients of determination. When fitting the data with the RK model, parameter C had a very low impact on the fitting. For this reason it can be kept constant to zero, as also confirmed by Askalany et al. [8] in the case of pure IL.

Table 11: Parameters of RK model and coefficients of determination for water sorption on [Cho][OAc] at different temperatures.

T [K]	A [-]	B [-]	C [-]	R^2
298.25	-13.542	12.421	0.000	0.999
303.25	-12.685	11.299	0.000	0.999
308.35	-12.107	10.611	0.000	1.000
318.55	-11.272	9.457	0.000	0.999
328.75	-10.419	8.114	0.000	0.999
333.85	-9.893	7.575	0.000	0.999
344.15	-9.526	7.257	0.000	0.999
349.55	-9.214	6.758	0.000	1.000

As demonstrated by the R^2 values in the table, the RK model is also capable to provide an excellent fit of the experimental data, even slightly better than the GAB model. When plotted against temperature, A and B parameters show a clear linear trend as depicted in Figure 5. Table 12 reports slopes, intercepts and coefficients of determination for the linearized A and B parameters.

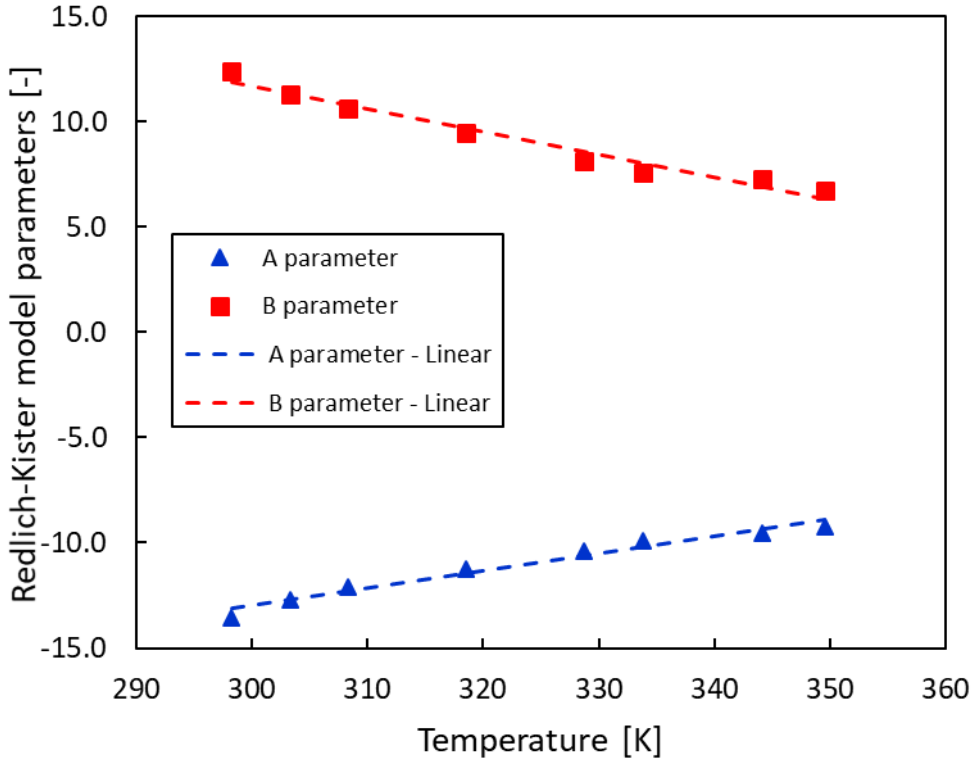

Figure 5: Parameters of RK model against temperature with linear trends displayed.

Table 12: Coefficients of linear temperature-dependent parameters of RK model.
$A = A_0 + A_1 \cdot T$; $B = B_0 + B_1 \cdot T$

A parameter			B parameter		
A_0 [-]	A_1 [K^{-1}]	R^2	B_0 [-]	B_1 [K^{-1}]	R^2
-37.492	0.082	0.971	43.885	-0.107	0.964

3.4 Prediction of excess properties with the Redlich-Kister model

With a linear temperature-dependent approach for A and B parameters of the RK model and fixing *C=0*, the molar excess Gibbs energy difference can be expressed as:

$$\Delta g^{EX} = R \cdot T \cdot x_W \cdot (1 - x_W) \cdot [A_0 + A_1 \cdot T + B_0 \cdot (2 \cdot x_W - 1) + B_1 \cdot T \cdot (2 \cdot x_W - 1)] \quad (17)$$

Eq. (17) can be directly applied to calculate the additional molar excess properties according to the following thermodynamic relations:

$$\frac{\partial(\Delta g^{EX}/T)}{\partial T} = -\frac{\Delta h^{EX}}{T^2} \quad (18)$$

$$\frac{\partial \Delta g^{EX}}{\partial T} = -\Delta s^{EX} \quad (19)$$

The resulting molar excess enthalpy and entropy differences are reported in Eqns (20−21):

$$\Delta h^{EX} = -R \cdot T^2 \cdot x_W \cdot (1 - x_W) \cdot [A_1 + B_1 \cdot (2 \cdot x_W - 1)] \quad (20)$$

$$\Delta s^{EX} = -R \cdot x_W \cdot (1 - x_W) \cdot [A_0 + 2 \cdot A_1 \cdot T + B_0 \cdot (2 \cdot x_W - 1) + 2 \cdot B_1 \cdot T \cdot (2 \cdot x_W - 1)] \quad (21)$$

Figure 6 shows the molar excess properties as a function of mole fraction of water at 298.25 K. The system water + [Cho][OAc] exhibits negative values of the excess Gibbs energy which indicates spontaneous water

sorption into the IL, which was also reported by Khan et al. [23] for several cholinium-based ionic liquids. The same authors showed that for [Cho][OAc] at 298.2 K and at $x_W = 0.66$ the estimated excess Gibbs energy was ≈ −4 kJ mol^{-1} and the excess enthalpy was ≈ −11.2 kJ mol^{-1} using the COSMO-RS model. From Figure 6 Δg^{EX} = −5.2 kJ mol^{-1} and Δh^{EX} = −7.9 kJ mol^{-1}, thus highlighting a qualitatively good agreement between RK and COSMO-RS models.

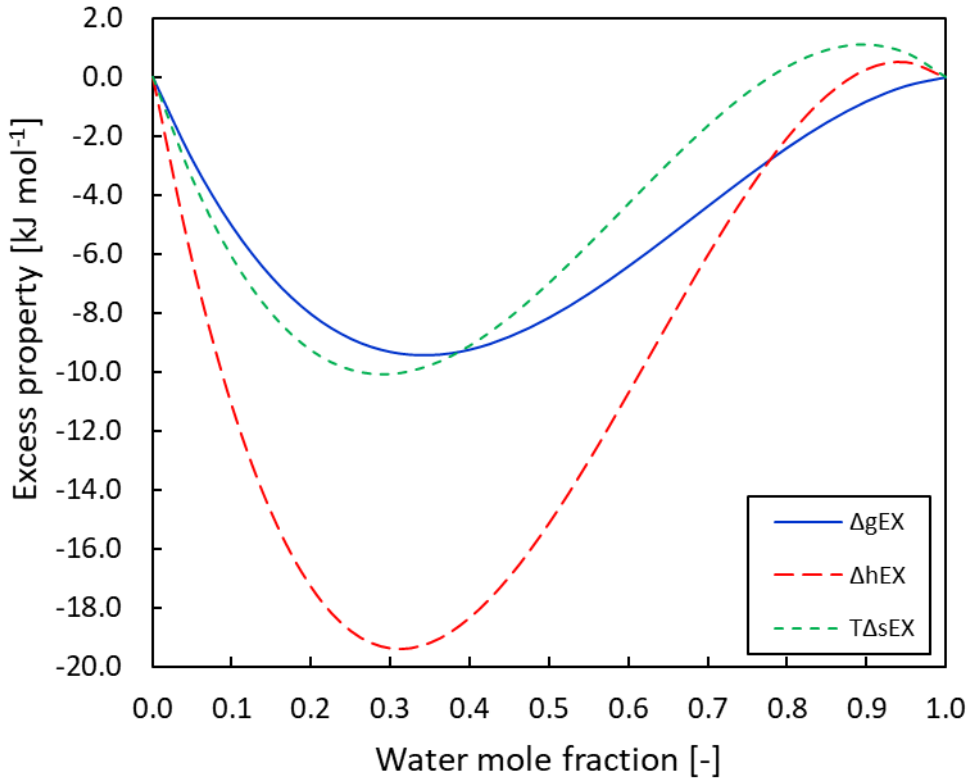

Figure 6: Excess molar properties against water mole fraction at 298.25 K for the system water + [Cho][OAc]. Curves are obtained using linear temperature-dependent parameters of the RK model.

4. Choline acetate as material for sorption chillers

One possible application for the investigated material is in sorption chillers using choline acetate as sorbent and water as refrigerant. A description of sorption cooling processes can be found in detail elsewhere [36–38]. The performance of a fluid-refrigerant working pair can be estimated from the thermodynamic cycle calculated by using the equilibrium data. The thermodynamic cycle ultimately leads to the identification of the Coefficient Of Performance (*COP*) [39,40]:

$$COP = \frac{Q_{ev}}{Q_{des}+Q_{ph}} \tag{22}$$

with

$$Q_{ph} = W_1 c_{p,w}(T_2 - T_1) + c_{p,IL}(T_2 - T_1) \tag{23}$$

$$Q_{des} = c_{p,IL}(T_3 - T_2) + \frac{W_2 - W_3}{2} c_{p,w}(T_3 - T_2) + \int_{W_2}^{W_3} h_{ads} dW \tag{24}$$

$$Q_{ev} = (W_1 - W_4)(L_w|_{T_{ev}} - c_{p,w}(T_1 - T_{ev})) \tag{25}$$

In the above Eqns (22–25) $W_{i,\,with\ i=1:4}$ is the adsorption uptake from the GAB isotherm (g_W g_{IL}^{-1}) relative to the specific thermodynamic cycle transformation where 1→2 is the isosteric heating, 2→3 is the isobaric desorption, 3→4 is the isosteric cooling and 4→1 is the isobaric adsorption [41], L_w is the latent heat of vaporization of water (kJ kg^{-1}), $c_{p,i}$ is the specific heat capacity of either water or IL (kJ kg^{-1} K^{-1}) and T_{ev} is the evaporation temperature of water (K). The specific heat capacity of choline acetate has not been reported in the literature yet and was estimated at 2.0 kJ kg^{-1} K^{-1}. The estimation is based on values reported by

Paulechka et al. [42] for imidazolium ionic liquids that ranged 1.3−1.9 kJ kg^{-1} K^{-1}. The heat capacity of choline chloride is 1.4 kJ kg^{-1} K^{-1} [43]. Moreover, molten sodium chloride has a specific heat of 1.0 kJ kg^{-1} K^{-1} [44]. The isosteric heat of adsorption h_{ads} (kJ kg^{-1}) can be obtained from the Clausius-Clapeyron relation:

$$h_{ads} = -\frac{RT^2}{MW_W}\left(\frac{\partial \ln(P)}{\partial T}\right)_q \tag{26}$$

where R is the universal gas constant (J mol^{-1} K^{-1}), MW_W is the molar mass of water (g mol^{-1}) and the partial derivative $dln(P)/dT$ is obtained from the GAB isotherm model, which can be solved with respect to the pressure P (bar) providing the following expression:

$$P = \frac{P^S \cdot \left(2 \cdot W - C \cdot W + C \cdot W_m - \sqrt{C} \cdot \sqrt{4 \cdot W \cdot W_m + C \cdot W^2 + C \cdot W_m^2 - 2 \cdot C \cdot W \cdot W_m}\right)}{2 \cdot (K \cdot W - C \cdot K \cdot W)} \tag{27}$$

where the saturation pressure of water P^S (bar) is expressed by the Antoine's relation due to its temperature dependency and C is defined by the Arrhenius-type expression: $C = C_0 \exp\left(-\frac{E_a}{RT}\right)$. The four regressed parameters W_m, C_0, K and E_a are given in the above section 3.2.

The COP was mapped for a range of evaporator temperatures between 5°C and 16°C and different heat source temperatures between 50°C and 80°C, as depicted in Figure 7(a) for choline acetate and in Figure 7(b) for silica gel [45]. It can be seen that the system choline acetate/water shows very high COP > 0.8 for heat sources of 65°C and higher. Here, the high COP can even be maintained for cooling temperatures as low as 5°C, where the COP drops only for heat source temperatures below 60°C. The comparison between silica gel and choline acetate in Figure 7 shows that the COP of choline acetate is up to 10% higher than silica gel for almost all the reported conditions.

Xu et al. [46] presented an experimental study on a lithium bromide/water absorption chiller that achieves a COP of 0.7 at 95°C providing chilled water at 9°C. Li and Sumathy [47] reported a COP in the range of 0.05−0.56 for heat source temperatures of 75−100°C using an absorption air conditioning system with lithium bromide/water and considering T_{ev} = 7°C and T_{cond} = 29.5°C. Compared with these literature benchmarks, the choline acetate/water pair achieves exceptional COP ≈ 0.75−0.83 for heat sources of 55−80°C, T_{ev} = 6.7°C and T_{cond} = 25°C (Figure 7(a)).

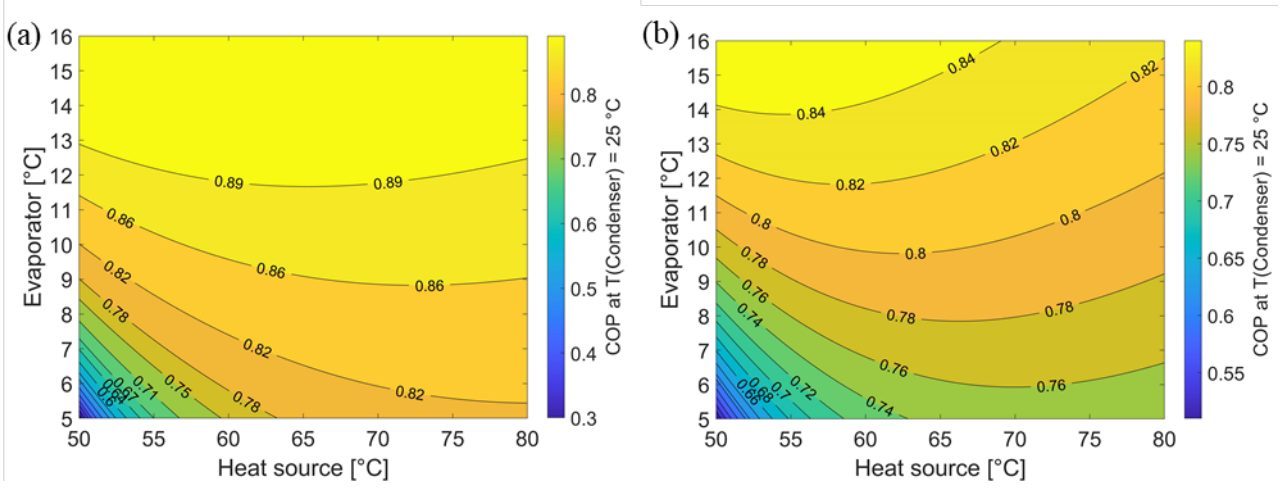

Figure 7: COP values for the system water + [Cho][OAc] (a) and Siogel silica gel from [45] (b) at different evaporator and heat source temperatures. The condenser temperature is fixed at 25°C.

5. Conclusion

In this work water sorption equilibria on choline acetate ionic liquid were measured with the use of a dynamic vapour sorption system. A total of eight temperatures (298.25, 303.25, 308.35, 318.55, 328.75, 333.85, 344.15 and 349.55 K) were investigated and a type III isotherm was observed in the entire range of temperatures. Exceptional water uptakes of above 3.5 g_W g_{IL}^{-1} were registered at 90% of relative humidity, demonstrating a

prospective for utilization in temperature-swing sorption heat transformers. It was found that the water uptake increased from 45.4°C to 55.6°C, denoting the phase transition of [Cho][OAc] from solid to liquid. This phenomenon was also confirmed by the analysis of the Gibbs energy difference between the absorbed state and the water saturation state resulting in two distinct characteristic curves at temperatures below and above the IL melting point.
Both the Guggenheim-Anderson-de Boer adsorption isotherm model and the Redlich-Kister excess Gibbs energy model provided an excellent description of the water sorption equilibria. In the RK model parameters showed a regular temperature dependence, enabling the calculation of excess enthalpy and excess entropy. A thermodynamic cycle analysis was carried out to assess the material suitability for sorption chillers with heat source temperatures in the range 50−80°C. The results indicated that the system choline acetate/water can achieve high COP of up to 0.8 even at 5°C evaporator temperature with a heat source temperature higher than 65°C, overcoming the sorbent benchmark performances and making it suitable for sorption cooling.

References

[1] Yu N, Wang RZ, Wang LW. Sorption thermal storage for solar energy. Progress in Energy and Combustion Science 2013;39:489–514. https://doi.org/10.1016/j.pecs.2013.05.004.

[2] Santori G, Frazzica A, Freni A, Galieni M, Bonaccorsi L, Polonara F, et al. Optimization and testing on an adsorption dishwasher. Energy 2013;50:170–6. https://doi.org/10.1016/j.energy.2012.11.031.

[3] Santori G, Luberti M. Thermodynamics of thermally-driven adsorption compression. Sustainable Materials and Technologies 2016;10:1–9. https://doi.org/10.1016/j.susmat.2016.09.001.

[4] Cranston J, Askalany A, Santori G. Efficient drying in washer dryers by combining sorption and heat pumping. Energy 2019;183:683–92. https://doi.org/10.1016/j.energy.2019.06.141.

[5] Grekova AD, Gordeeva LG, Lu Z, Wang R, Aristov YI. Composite "LiCl/MWCNT" as advanced water sorbent for thermal energy storage: Sorption dynamics. Solar Energy Materials and Solar Cells 2018;176:273–9. https://doi.org/10.1016/j.solmat.2017.12.011.

[6] Tokarev MM, Gordeeva LG, Grekova AD, Aristov YI. Adsorption cycle "heat from cold" for upgrading the ambient heat: The testing a lab-scale prototype with the composite sorbent CaClBr/silica. Applied Energy 2018;211:136–45. https://doi.org/10.1016/j.apenergy.2017.11.015.

[7] Shahzad MW, Ng KC, Thu K. Future sustainable desalination using waste heat: Kudos to thermodynamic synergy. Environmental Science: Water Research and Technology 2016;2:206–12. https://doi.org/10.1039/c5ew00217f.

[8] Askalany AA, Freni A, Santori G. Supported ionic liquid water sorbent for high throughput desalination and drying. Desalination 2019;452:258–64. https://doi.org/10.1016/j.desal.2018.11.002.

[9] Restuccia G, Freni A, Vasta S, Aristov Y. Selective water sorbent for solid sorption chiller: Experimental results and modelling. International Journal of Refrigeration, vol. 27, 2004, p. 284–93. https://doi.org/10.1016/j.ijrefrig.2003.09.003.

[10] Tu YD, Wang RZ, Ge TS. New concept of desiccant-enhanced heat pump. Energy Conversion and Management 2018;156:568–74. https://doi.org/10.1016/j.enconman.2017.11.068.

[11] Radakovitsch FR, Jess A. Gas dehydration using the ionic liquid [EMIM][MeSO3] supported on silica gel - structural and water vapor sorption properties. Chemical Engineering Journal 2020:124689. https://doi.org/10.1016/j.cej.2020.124689.

[12] Boman DB, Hoysall DC, Staedter MA, Goyal A, Ponkala MJ, Garimella S. A method for comparison of absorption heat pump working pairs. International Journal of Refrigeration 2017;77:149–75. https://doi.org/10.1016/j.ijrefrig.2017.02.023.

[13] Cao Y, Sun X, Chen Y, Mu T. Water sorption in amino acid ionic liquids: Kinetic, mechanism, and correlations between hygroscopicity and solvatochromic parameters. ACS Sustainable Chemistry and Engineering 2014;2:138–48. https://doi.org/10.1021/sc4003246.

[14] Chen Y, Cao Y, Mu T. A new application of acetate-based ionic liquids: Potential usage as drying materials. Chemical Engineering and Technology 2014;37:527–34. https://doi.org/10.1002/ceat.201300583.

[15] Di Francesco F, Calisi N, Creatini M, Melai B, Salvo P, Chiappe C. Water sorption by anhydrous ionic liquids. Green Chemistry 2011;13:1712–7. https://doi.org/10.1039/c1gc15080d.

[16] Cao Y, Chen Y, Sun X, Zhang Z, Mu T. Water sorption in ionic liquids: Kinetics, mechanisms and hydrophilicity. Physical Chemistry Chemical Physics 2012;14:12252–62. https://doi.org/10.1039/c2cp41798g.

[17] Neves CMSS, Lemus J, Freire MG, Palomar J, Coutinho JAP. Enhancing the adsorption of ionic liquids onto activated carbon by the addition of inorganic salts. Chemical Engineering Journal 2014;252:305–10. https://doi.org/10.1016/j.cej.2014.05.009.

[18] Brennecke JF, Maginn EJ. Ionic liquids: Innovative fluids for Chemical Processing. AIChE Journal 2001;47:2384–2389. https://doi.org/10.1002/aic.690471102.

[19] Rogers RD, Seddon KR. Ionic Liquids - Solvents of the Future? Science 2003;302:792–3. https://doi.org/10.1126/science.1090313.

[20] Römich C, Merkel NC, Valbonesi A, Schaber K, Sauer S, Schubert TJS. Thermodynamic properties of binary mixtures of water and room-temperature ionic liquids: Vapor pressures, heat capacities, densities, and viscosities of water + 1-ethyl-3-methylimidazolium acetate and water + diethylmethylammonium methane sulfonate. Journal of Chemical and Engineering Data 2012;57:2258–64. https://doi.org/10.1021/je300132e.

[21] Merkel N, Weber C, Faust M, Schaber K. Influence of anion and cation on the vapor pressure of binary mixtures of water+ionic liquid and on the thermal stability of the ionic liquid. Fluid Phase Equilibria 2015;394:29–37. https://doi.org/10.1016/j.fluid.2015.03.001.

[22] Constantinescu D, Schaber K, Agel F, Klingele MH, Schubert TJS. Viscosities, vapor pressures, and excess enthalpies of choline lactate + water, choline glycolate + water, and choline methanesulfonate + water systems. Journal of Chemical and Engineering Data 2007;52:1280–5. https://doi.org/10.1021/je7000232.

[23] Khan I, Kurnia KA, Sintra TE, Saraiva JA, Pinho SP, Coutinho JAP. Assessing the activity coefficients of water in cholinium-based ionic liquids: Experimental measurements and COSMO-RS modeling. Fluid Phase Equilibria 2014;361:16–22. https://doi.org/10.1016/j.fluid.2013.10.032.

[24] Colomines G, Decaen P, Lourdin D, Leroy E. Biofriendly ionic liquids for starch plasticization: A screening approach. RSC Advances 2016;6:90331–7. https://doi.org/10.1039/c6ra16573g.

[25] Fukaya Y, Iizuka Y, Sekikawa K, Ohno H. Bio ionic liquids: Room temperature ionic liquids composed wholly of biomaterials. Green Chemistry 2007;9:1155–7. https://doi.org/10.1039/b706571j.

[26] Cheng F, Wang H, Chatel G, Gurau G, Rogers RD. Facile pulping of lignocellulosic biomass using choline acetate. Bioresource Technology 2014;164:394–401. https://doi.org/10.1016/j.biortech.2014.05.016.

[27] Lopes JM, Paninho AB, Môlho MF, Nunes AVM, Rocha A, Lourenço NMT, et al. Biocompatible choline based ionic salts: Solubility in short-chain alcohols. Journal of Chemical Thermodynamics 2013;67:99–105. https://doi.org/10.1016/j.jct.2013.07.025.

[28] Muhammad N, Hossain MI, Man Z, El-Harbawi M, Bustam MA, Noaman YA, et al. Synthesis and physical properties of choline carboxylate ionic liquids. Journal of Chemical and Engineering Data 2012;57:2191–6. https://doi.org/10.1021/je300086w.

[29] Zhang Q, Benoit M, Dea Oliveiraa Vigier K, Barrault J, Jérŏme F. Green and inexpensive choline-derived solvents for cellulose decrystallization. Chemistry - A European Journal 2012;18:1043–6. https://doi.org/10.1002/chem.201103271.

[30] Fernandez L, Silva LP, Martins MAR, Ferreira O, Ortega J, Pinho SP, et al. Indirect assessment of the fusion properties of choline chloride from solid-liquid equilibria data. Fluid Phase Equilibria 2017;448:9–14. https://doi.org/10.1016/j.fluid.2017.03.015.

[31] Sigma-Aldrich. Choline acetate, 2019. Available online at https://www.sigmaaldrich.com/catalog/product/aldrich/670189?lang=en&region=GB.

[32] Surface Measurement Systems. DVS Adventure, 2016. Available online at http://surfacemeasurementsystems.com/wp-content/uploads/2016/06/DVS_Adventure_Brochure_final_digital_updated_12July2016.pdf

[33] Glass SV, Boardman CR, Thybring EE, Zelinka SL. Quantifying and reducing errors in equilibrium moisture content measurements with dynamic vapor sorption (DVS) experiments. Wood Science and Technology 2018;52:909–27. https://doi.org/10.1007/s00226-018-1007-0.

[34] Aristov Y. Concept of adsorbent optimal for adsorptive cooling/heating. Applied Thermal Engineering 2014;72:166–75. https://doi.org/10.1016/j.applthermaleng.2014.04.077.

[35] Bratasz L, Kozłowska A, Kozłowski R. Analysis of water adsorption by wood using the Guggenheim-Anderson-de Boer equation. European Journal of Wood and Wood Products 2012;70:445–51. https://doi.org/10.1007/s00107-011-0571-x.

[36] Olkis C, Brandani S, Santori G. Cycle and performance analysis of a small-scale adsorption heat transformer for desalination and cooling applications. Chemical Engineering Journal 2019;378. https://doi.org/10.1016/j.cej.2019.122104.

[37] Luberti M, di Santis C, Santori G. Ammonia/ethanol mixture for adsorption refrigeration. Energies 2020;13. https://doi.org/10.3390/en13040983.

[38] Gebreslassie BH, Groll EA, Garimella S v. Multi-objective optimization of sustainable single-effect water/Lithium Bromide absorption cycle. Renewable Energy 2012;46:100–10. https://doi.org/10.1016/j.renene.2012.03.023.

[39] Santori G, di Santis C. Optimal fluids for adsorptive cooling and heating. Sustainable Materials and Technologies 2017;12:52–61. https://doi.org/10.1016/j.susmat.2017.04.005.

[40] Critoph RE. Performance limitations of adsorption cycles for solar cooling. Solar Energy 1988;41:21–31. https://doi.org/10.1016/0038-092X(88)90111-9.

[41] Askalany A, Olkis C, Bramanti E, Lapshin D, Calabrese L, Proverbio E, et al. Silica-Supported Ionic Liquids for Heat-Powered Sorption Desalination. ACS Applied Materials and Interfaces 2019;11:36497–505. https://doi.org/10.1021/acsami.9b07602.

[42] Paulechka YU, Kabo AG, Blokhin A v., Kabo GJ, Shevelyova MP. Heat capacity of ionic liquids: Experimental determination and correlations with molar volume. Journal of Chemical and Engineering Data 2010;55:2719–24. https://doi.org/10.1021/je900974u.

[43] Chemat F, Anjum H, Shariff AM, Kumar P, Murugesan T. Thermal and physical properties of (Choline chloride + urea + l-arginine) deep eutectic solvents. Journal of Molecular Liquids 2016;218:301–8. https://doi.org/10.1016/j.molliq.2016.02.062.

[44] Stull DR, Prophet H. JANAF Thermochemical Tables. US National Bureau of Standards, Washington DC, 1971. Available online at https://janaf.nist.gov/

[45] Sapienza A, Velte A, Girnik I, Frazzica A, Füldner G, Schnabel L, et al. "Water - Silica Siogel" working pair for adsorption chillers: Adsorption equilibrium and dynamics. Renewable Energy 2017;110:40–6. https://doi.org/10.1016/j.renene.2016.09.065.

[46] Xu ZY, Wang RZ, Wang HB. Experimental evaluation of a variable effect LiBr-water absorption chiller designed for high-efficient solar cooling system. International Journal of Refrigeration 2015;59:135–43. https://doi.org/10.1016/j.ijrefrig.2015.07.019.

[47] Li ZF, Sumathy K. Simulation of a solar absorption air conditioning system. Energy Conversion & Management 2001;42:313−327. https://doi.org/10.1016/S0196-8904(00)00057-1.